Sensitivity Analysis of Inductive Power Transfer Systems With Voltage-Fed Compensation Topologies

Lu, J.; Zhu, G.; Wang, Huai; Lu, F.; Jiang, J.; Mi, C. C.

Sensitivity Analysis of Inductive Power Transfer Systems with Voltage-Fed Compensation Topologies

Jianghua Lu, *Student Member, IEEE*, Guorong Zhu, *Senior Member, IEEE*, Huai Wang, *Senior Member, IEEE*, Fei Lu, *Member, IEEE*, Jin Jiang, *Fellow, IEEE*, and Chunting Chris Mi, *Fellow, IEEE*

Abstract—The output characteristics and the transfer efficiencies of Inductive Power Transfer (IPT) systems are affected by the variation of parameters such as, but not limited to, variable load, misalignment between the primary and secondary coils, and resonance frequency detuning. This paper first analyzes the resonant conditions of all voltage-fed compensation topologies in IPT systems to achieve the load-independent voltage transfer characteristic at load-independent Zero Phase Angle (ZPA) frequency. With these conditions, the parameters sensitivity to the key performance factors of the S-SP, LCC-S, LCC-P, and double-sided LCC compensated IPT systems are systematically investigated when considering the losses in coils and compensation networks. Comparisons of the quantitative sensitivity analysis and experimental results for all IPT systems are made in terms of the voltage transfer ratio and efficiency. These analyses can provide guidance for the selection of superior compensation networks to minimize the additional converter effort and simplify the control algorithm of closed-loop IPT systems.

Index Terms—Compensation topology, constant voltage, inductive power transfer, parametric uncertainty, sensitivity, Zero Phase Angle (ZPA).

I. INTRODUCTION

INDUCTIVE power transfer (IPT) technology [1], [2] using magnetic coupling can transfer power from several milliwatts to hundreds of kilowatts with transfer distances from a few millimeters to several meters. The IPT technology has gained its wide acceptance across a range of applications such as electronic devices, wearable/implantable electronics, home appliances, and electric vehicles (EVs).

In IPT applications, several compensation networks in both primary (transmitter) and secondary (receiver) sides have been

J. Lu and G. Zhu are with the School of Automation, Wuhan University of Technology, Wuhan 430070, China (e-mail: tri_ljh@whut.edu.cn; zhgr_55@whut.edu.cn).

H. Wang is with the Department of Energy Technology, Aalborg University, DK-9220 Aalborg, Denmark (e-mail: hwa@et.aau.dk).

F. Lu is with the Department of Electrical and Computer Engineering, Drexel University, Philadelphia, PA 19104, USA (e-mail: fei.lu@drexel.edu).

J. Jiang is with the Department of Electrical and Computer Engineering, The University of Western Ontario, London, ON N6A 3K7, Canada (e-mail: jjiang@eng.uwo.ca).

C. Mi is with the Department of Electrical and Computer Engineering, San Diego State University, San Diego, CA 92182, USA (e-mail: cmi@sdsu.edu).

proposed and are usually used to achieve and/or improve the following one or more characteristics:

1) *Near zero input reactive power*. It is desirable for the primary inverter in IPT system to have Zero Phase Angle (ZPA) operating condition between the inverter output voltage and current. In such case, there is no reactive power circulating in the loop, which can minimize the Volt-Ampere (VA) rating of the power supply, increase the transfer power to the load, and make it easy to ensure Zero Voltage Switching (ZVS) [3], [4]. For example, ZPA operation is achieved for the series-series (S-S) compensation topology when the primary and secondary compensation capacitors are used to resonant with the self-inductance of the primary and secondary coils respectively [5].

2) *Constant current and/or constant voltage output*. A constant charging current for LED (Light Emitting Diode) application and a charging profile with constant current/constant voltage for EV and electric bicycle charger, regardless of the value of the load resistance, are the most important characteristics for IPT system. Among the approaches for achieving load-independent current output and/or load-independent voltage output, the method of designing special tuning conditions for compensation topology [4], [6] has the advantages of higher efficiency and lower cost compared with a back-end DC/DC converter [7] and is free from frequency bifurcation phenomenon and wireless data communication link between secondary and primary sides for the variable frequency control method [8]. The load-independent current output feature has been analyzed for the S-S [4], [9]-[12], series-parallel (S-P) [12], LCC-parallel (LCC-P) [4], and double-sided LCC [4], [6], [13], [14] compensation topologies by designing special tuning methods. And the load-independent voltage transfer characteristic is investigated for the S-S [4], [9], [15], [16], S-P [5], [16], S-SP [4], [17], LCC-series (LCC-S) [4], S-CLC [18], and double-sided LCC topologies [13], [14]. In [19], a general method that models a resonant circuit as gyrators in series is proposed. This method can be used to analyze the load-independent current output or voltage output characteristic of any compensation topologies in IPT system. Further, under the condition of achieving load-independent current output characteristic, input ZPA operations are analyzed for S-S [4], [5], [9],

[12] and double-sided LCC [6], [13] topologies. And the ZPA operating conditions are also achieved for the S-P [5], S-SP [4], S-CLC [18], and double-sided LCC [13] topologies in constant voltage output mode.

3) *High and steady efficiency*. The Zero Voltage Switching (ZVS) operating condition can improve the efficiency of the H-bridge inverter using MOSFETs in primary side [6], [9], [20]. In addition, as stated before, ZPA operation can minimize the VA rating of the power supply and increase the transfer power to the load. So it should make a trade-off between the input phase angle as small as possible and the ZVS operating condition during the process of the entire charging profile. In [6] and [21], the ZPA operations are analyzed for the double-sided LCC and S-LCC compensation topologies respectively. Furthermore, under the condition of achieving ZPA, ZVS operations are achieved by slightly changing the value of a certain compensation capacitor. Additionally, designing an appropriate compensation topology is also an effective method to obtain high efficiency. The higher and stable efficiency can be achieved for the double-sided LCC compensation topology compared with S-S topology [22]. In [23], series-parallel resonant can achieve higher efficiency over the full range of coupling and loading compared with series resonant.

4) *Less sensitivity to the variable parameters*. The capacitance value of the compensation capacitor may be changed with the different operational time and environment [24], [25]. And the capacitor will suffer from the inevitable manufacturing tolerance. On the other hand, the self-inductances of the primary and secondary coils and mutual inductance between the two coils will change along with the misalignment [26], [27]. So, the natural resonant frequency of the resonant tank circuit will change along with the variable capacitance and/or variable inductance. Besides, the coupling coefficient will be varied with the relative position between the primary and secondary coils, and the battery load resistance also changes along with the battery charging profile. These inevitable variations of the frequency, coupling, and load may have negative effect on the voltage and current transfer characteristics and efficiency of the IPT system. Therefore, a superior compensation network with less sensitivity to the variable parameters is necessary. In [24], the sensitivity of the output power and efficiency to parameter variations of the compensation components in the double-sided LCC compensated IPT system are analyzed. The output current characteristics for the P-S, primary parallel/series and secondary series (PS-S), double-sided LCL, and LCC-P compensation topologies to the variations of coupling and load are analyzed [10]. In [10], it is concluded that the PS-S topology is the least output current fluctuation over wide range of coupling and load variations.

For an open-loop IPT system, what we desire to accomplish is not only minimize the output voltage and/or current fluctuation, but also achieve higher and steady efficiency under taking into account the variations of the input voltage, resonant frequency, coupling, and load. In this case, a closed-loop IPT systems with minimizing the additional converter effort and simplifying the control algorithm can easily be designed over the entire range of charging profile. So it is necessary to systematically investigate the parametric uncertainty to the key performance factors and compare the robust of the different compensation topologies.

This paper mainly focuses on the comprehensive evaluation of the voltage-fed S-S, S-P, S-SP, LCC-S, LCC-P, and double-sided LCC compensation topologies in IPT system. When the parasitic resistances of the compensation components are neglected, all compensation networks are modeled as cascade combinations of multistages T-circuit to investigate the load-independent voltage transfer characteristics and load-independent ZPA operating conditions. Under these conditions, the influences of the variations of the coupling, load, and frequency on the output voltage and transfer efficiency are analyzed when the coils and compensation networks have the parasitic resistances. Finally, prototypes of 3-kW S-SP, LCC-S, LCC-P, and double-sided LCC compensated IPT systems are implemented to verify the sensitivity analyses.

The remainder of the paper is organized as follows. Section II investigates the equivalent circuits and resonant conditions of the S-S, S-P, S-SP, LCC-S, LCC-P, and double-sided LCC compensation topologies for achieving load-independent voltage outputs with ZPA conditions. Based on the analysis in Section II, the system parameters are designed in Section III, additionally, the sensitivity of the variations of the coupling, load, and frequency on the output voltage and efficiency for all IPT systems are investigated when the resonant components of the system have parasitic resistances. Section IV presents the experimental results of 3-kW IPT systems, followed by the conclusion in Section V.

II. LOAD-INDEPENDENT VOLTAGE TRANSFER CHARACTERISTIC WITH LOAD-INDEPENDENT ZPA

A general IPT system is shown in Fig. 1, which is composed of a full-bridge inverter, a high-order resonant tank network, a rectifier with capacitor (or inductor) filter, and the load. The resonant tank is composed of compensation networks in both primary and secondary sides and a loosely coupled transformer (LCT). L_p (and/or C_p) and L_s (and/or C_s) represent the compensation inductors (capacitors) in primary and secondary sides respectively. L_{pS} and L_{sS} are the self-inductances of the primary and secondary coils, and M is the mutual inductance between the two coils. $\mathbf{V}_{AB}$ and $\mathbf{I}_{AB}$ represent the phasor forms of the input voltage and current of the resonant tank and $\mathbf{V}_{ab}$ and $\mathbf{I}_{ab}$ are its output voltage and current. The equivalent circuits referred to the primary side for some widely-used voltage-fed compensation topologies (S-S, S-P, S-SP, LCC-S, LCC-P, and double-sided LCC) are shown in Fig. 2(a) to 2(f). It should be pointed out that the parallel-parallel (P-P), the parallel-series (P-S), and the PS-S compensation topologies are not analyzed in this paper because the voltage of the primary parallel compensation capacitor rises to source voltage immediately when the voltage polarity changes, causing instant large current and impairing capacitor lifespan. As shown in Fig. 2, a frequency-domain equivalent circuit is adopted
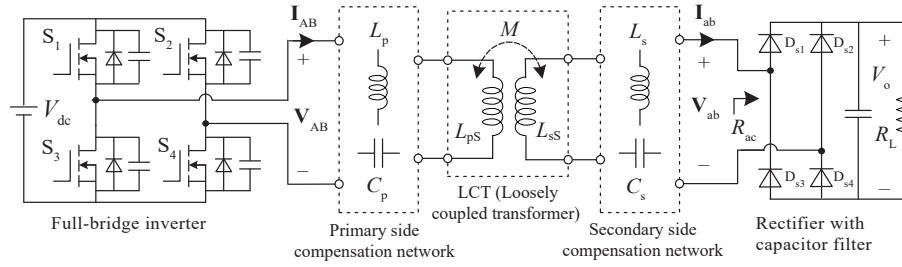
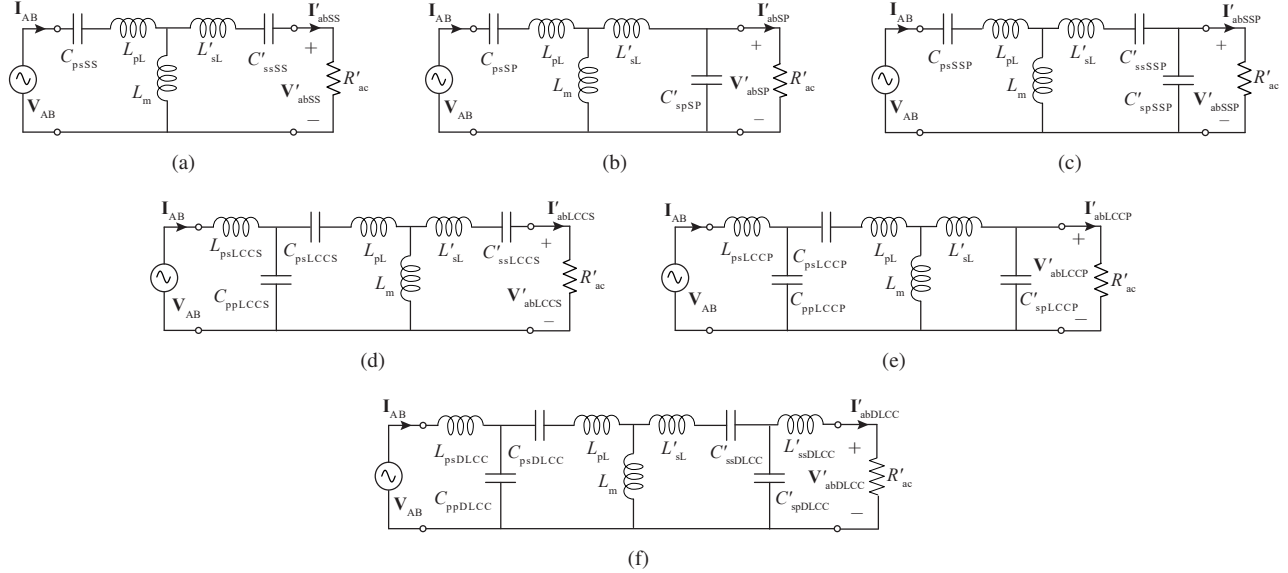Fig. 1. A general inductive power transfer system.

Fig. 2. Equivalent circuits referred to primary side of the (a) S-S, (b) S-P, (c) S-SP, (d) LCC-S, (e) LCC-P, and (f) double-sided LCC topologies. The unified nomenclature of the compensation elements are presented. $C_{\mathrm{ps}x}$ (the first subscript "p" represents primary side, the "s" represents series connection, and subscript "x" represents the different topologies) is the series compensation capacitor at the primary side. And $L_{\mathrm{ss}x}$ represents the series compensation inductor at the secondary side.

and only the fundamental component is considered here for simplicity, and the LCT is modeled as its T-model. The first-order RMS value of the input voltage can be expressed as $V_{\mathrm{AB}} = 2\sqrt{2}V_{\mathrm{dc}}/\pi$ and the equivalent ac resistance for the rectifier with capacitor (or inductor) output filter is given by $R_{\mathrm{ac}} = 8R_{\mathrm{L}}/\pi^2$ (or $R_{\mathrm{ac}} = \pi^2 R_{\mathrm{L}}/8$) [28]. The rectifier with inductor filter should be selected for the S-P, S-SP, and LCC-P topologies. However, the S-S, LCC-S, and double-sided LCC topologies apply the rectifier with capacitor filter. L_{pL} and L_{sL} are the leakage inductance of the primary and secondary coils, and L_{m} represents magnetizing inductance. Here and in the later section, the apostrophe symbol " $'$ " indicates the corresponding variables of the secondary side converted to primary side. In addition, the unified nomenclature of the compensation components is presented in here. $C_{\mathrm{ps}x}$ (the first subscript "p" represents primary side, the subscript "s" represents series connection, and the last subscript "x" represents the different topologies) is the series compensation capacitors at the primary side for a certain compensation topology. And $L_{\mathrm{ss}x}$ represents the series compensation inductor at secondary side. For example, C_{ppDLCC} in Fig. 2(f) is the parallel connected compensation capacitor in primary side of the double-sided LCC compensation topology. In addition, $\mathbf{V}'_{\mathrm{ab}x}$ and $\mathbf{I}'_{\mathrm{ab}x}$ represent the output voltage and current of the different compensation topologies.

A. Load-independent voltage transfer ratio

In this paper, we focus on the sensitivity of the output voltages for all voltage-fed compensation topologies in IPT system to the variable parameters. In [14], a general modeling method for an arbitrary high-order resonant network is proposed, in which the resonant network is modeled as multiple T-circuits in series to analyze its load-independent voltage transfer characteristic. We can see that all compensation topologies shown in Fig. 2 are inherently high-order resonant networks. So the proposed method in [14] can be applied to analyze the load-independent voltage transfer characteristics of all compensation topologies. Among all compensation topologies, the double-sided LCC compensation topology shown in Fig. 2(f) has the highest degree of freedom. Thus, it is taken as an example to analyze the load-independent voltage transfer characteristic in detail. The analyses of other compensation topologies will be followed.

For constructing resonant T-circuit to analyze the load-independent voltage transfer characteristic, the series-connected capacitor and inductor branches of the double-sided LCC compensation topology shown in Fig. 2(f), i.e., C_{psDLCC} and L_{pL} are expressed by using L_{epDLCC} and C_{epDLCC}. In addition, L'_{sL} and C'_{ssDLCC} are equivalent to C'_{esDLCC} and L'_{esDLCC}. Then, the double-sided LCC compensation topology can be equivalent to Fig. 3, which is composed of three-stage
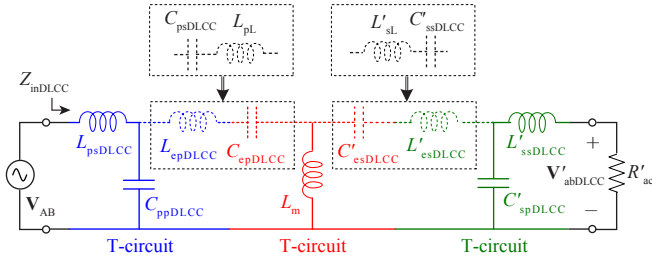
Fig. 3. Equivalent T-circuit of the double-sided LCC topology to obtain load-independent voltage transfer ratio.

T-circuit in series. The equivalent variables are expressed as

$$-\omega_{\mathrm{DLCC}}^2 L_{\mathrm{epDLCC}} + \frac{1}{C_{\mathrm{epDLCC}}} = -\omega_{\mathrm{DLCC}}^2 L_{\mathrm{pL}} + \frac{1}{C_{\mathrm{psDLCC}}}$$
$$-\omega_{\mathrm{DLCC}}^2 L'_{\mathrm{esDLCC}} + \frac{1}{C'_{\mathrm{esDLCC}}} = -\omega_{\mathrm{DLCC}}^2 L'_{\mathrm{sL}} + \frac{1}{C'_{\mathrm{ssDLCC}}} \quad (1)$$

where, ω_{DLCC} represents the resonant angular frequency of the double-sided LCC resonant tank.

According to the analysis of achieving load-independent voltage transfer characteristic for the T-circuit in [14], the resonant conditions of the equivalent T-circuit of the double-sided LCC compensation topology to achieve load-independent voltage transfer ratio are expressed as

$$\omega_{\mathrm{DLCC}}^2 = \frac{L_{\mathrm{psDLCC}} + L_{\mathrm{epDLCC}}}{L_{\mathrm{psDLCC}} L_{\mathrm{epDLCC}} C_{\mathrm{ppDLCC}}} = \frac{1}{L_{\mathrm{m}}\left(C_{\mathrm{epDLCC}} + C'_{\mathrm{esDLCC}}\right)}$$
$$= \frac{L'_{\mathrm{esDLCC}} + L'_{\mathrm{ssDLCC}}}{L'_{\mathrm{esDLCC}} L'_{\mathrm{ssDLCC}} C'_{\mathrm{spDLCC}}} \quad (2)$$

And, the corresponding load-independent voltage transfer ratio $\mathbf{G}_{\mathrm{DLCC}}$ ($\mathbf{G}_{\mathrm{DLCC}}$ is the ratio of the output voltage $\mathbf{V}'_{\mathrm{abDLCC}}$ to the input voltage $\mathbf{V}_{\mathrm{AB}}$) is calculated by

$$\mathbf{G}_{\mathrm{DLCC}} = \frac{\mathbf{V}'_{\mathrm{abDLCC}}}{\mathbf{V}_{\mathrm{AB}}}$$
$$= \left(-\frac{L_{\mathrm{epDLCC}}}{L_{\mathrm{psDLCC}}}\right)\left(-\frac{C_{\mathrm{epDLCC}}}{C'_{\mathrm{esDLCC}}}\right)\left(-\frac{L'_{\mathrm{ssDLCC}}}{L'_{\mathrm{esDLCC}}}\right) \quad (3)$$

The constant $\mathbf{V}'_{\mathrm{abDLCC}}$ can be achieved when the double-sided LCC compensation topology is driven by a constant voltage supply. And $\mathbf{V}'_{\mathrm{abDLCC}}$ lags $\mathbf{V}_{\mathrm{AB}}$ by 180 degrees.

Similarly, the S-S and LCC-S compensation topologies can be equivalent to one or more T-circuit in series, which are shown in Fig. 4(a) and 4(d). The S-P, S-SP, and LCC-P compensation topologies are equivalent to cascade connections of one or more T-circuit with a parallel capacitor, which are shown in Fig. 4(c), 4(b), and 4(e), respectively. Here, it should be noted that the output parallel capacitor does not affect the output voltage. So, we only need to analyze the voltage transfer characteristics of the equivalent T-circuits of all compensation topologies.

From Fig. 4, the equivalent variables, resonant conditions for achieving load-independent voltage transfer characteristic, and corresponding mathematical models of the load-independent voltage transfer ratio of the S-S, S-P, S-SP, LCC-S and LCC-P compensation topologies can be presented in Tab. I. From the last column of Tab. I, it can be seen that the voltage transfer ratios of all compensation topologies ($\mathbf{G}_{\mathrm{SS}}$, $\mathbf{G}_{\mathrm{SP}}$, $\mathbf{G}_{\mathrm{SSP}}$, $\mathbf{G}_{\mathrm{LCCS}}$, and $\mathbf{G}_{\mathrm{LCCP}}$) are independent of the load. And the output voltages of the S-P, S-SP, and LCC-S topologies
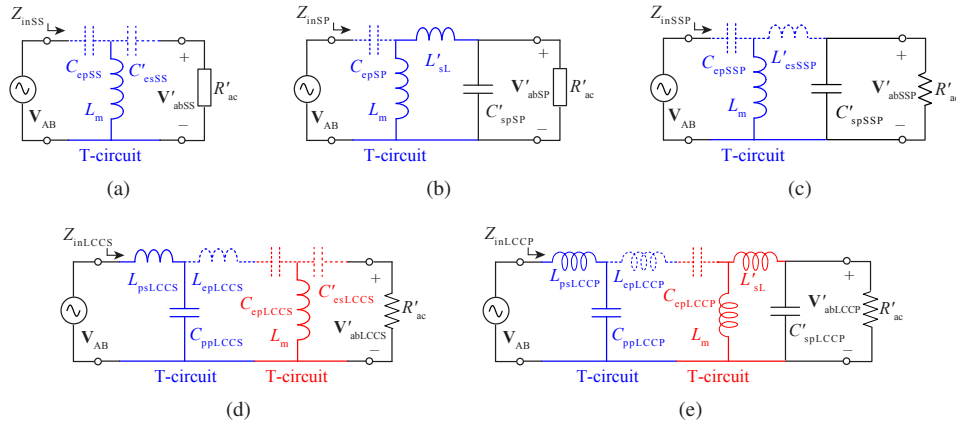
Fig. 4. Equivalent T-circuit of (a) S-S, (b) S-P, (c) S-SP, (d) LCC-S, and (e) LCC-P topologies.

$$Z_{\mathrm{inDLCC}} = \left(\left(\left(R'_{\mathrm{ac}} + j\omega_{\mathrm{DLCC}}L'_{\mathrm{ssDLCC}}\right) \| \frac{1}{j\omega_{\mathrm{DLCC}}C'_{\mathrm{spDLCC}}} + j\omega_{\mathrm{DLCC}}L'_{\mathrm{esDLCC}} + \frac{1}{j\omega_{\mathrm{DLCC}}C'_{\mathrm{esDLCC}}}\right) \| j\omega_{\mathrm{DLCC}}L_{\mathrm{m}}\right.$$
$$\left. + \frac{1}{j\omega_{\mathrm{DLCC}}C_{\mathrm{epDLCC}}} + j\omega_{\mathrm{DLCC}}L_{\mathrm{epDLCC}}\right) \| \frac{1}{j\omega_{\mathrm{DLCC}}C_{\mathrm{ppDLCC}}} + j\omega_{\mathrm{DLCC}}L_{\mathrm{psDLCC}}$$
$$= \mathrm{Re}\left(Z_{\mathrm{inDLCC}}\right) + j \cdot \mathrm{Im}\left(Z_{\mathrm{inDLCC}}\right) \quad (4)$$

$$\mathrm{Im}\left(Z_{\mathrm{inDLCC}}\right) = 0 \rightarrow$$
$$L_{\mathrm{epDLCC}}L'_{\mathrm{esDLCC}}C_{\mathrm{epDLCC}}C'_{\mathrm{esDLCC}}\left(C_{\mathrm{epDLCC}} + C'_{\mathrm{esDLCC}}\right) = L_{\mathrm{epDLCC}}L'_{\mathrm{ssDLCC}}C'_{\mathrm{spDLCC}}C_{\mathrm{epDLCC}}^2 + L'_{\mathrm{esDLCC}}L_{\mathrm{psDLCC}}C_{\mathrm{ppDLCC}}C'^2_{\mathrm{esDLCC}} \quad (5)$$

TABLE I
RESONANT CONDITIONS OF S-S, S-P, S-SP, LCC-S AND LCC-P TOPOLOGIES FOR ACHIEVING LOAD-INDEPENDENT VOLTAGE TRANSFER CHARACTERISTICS AND CORRESPONDING MATHEMATICAL MODELS OF LOAD-INDEPENDENT VOLTAGE TRANSFER RATIO.

	Equivalent Variables	Resonant condition	Voltage gain $G_x = \dfrac{V_{abx}}{V_{AB}}$
S-S	$\dfrac{1}{C_{epSS}} = -\omega_{SS}^2 L_{pL} + \dfrac{1}{C_{psSS}}$ $\dfrac{1}{C'_{esSS}} = -\omega_{SS}^2 L'_{sL} + \dfrac{1}{C'_{ssSS}}$	$\omega_{SS}^2 = \dfrac{1}{L_m(C_{epSS}+C'_{esSS})}$	$G_{SS} = -\dfrac{C_{epSS}}{C_{esSS}}$
S-P	$\dfrac{1}{C_{epSP}} = -\omega_{SP}^2 L_{pL} + \dfrac{1}{C_{psSP}}$	$\omega_{SP}^2 = \dfrac{L_m + L'_{sL}}{C_{epSP} L_m L'_{sL}}$	$G_{SP} = \dfrac{L_m + L'_{sL}}{L_m} = \dfrac{1}{k}$
S-SP	$\dfrac{1}{C_{epSSP}} = -\omega_{SSP}^2 L_{pL} + \dfrac{1}{C_{psSSP}}$ $-\omega_{SSP}^2 L'_{esSSP} = -\omega_{SSP}^2 L'_{sL} + \dfrac{1}{C'_{ssSSP}}$	$\omega_{SSP}^2 = \dfrac{L_m + L'_{esSSP}}{L_m L'_{esSSP} C_{epSSP}}$	$G_{SSP} = \dfrac{L_m + L'_{esSSP}}{L_m}$
LCC-S	$-\omega_{LCCS}^2 L_{epLCCS} + \dfrac{1}{C_{epLCCS}} = -\omega_{LCCS}^2 L_{pL} + \dfrac{1}{C_{psLCCS}}$ $\dfrac{1}{C'_{esLCCS}} = -\omega_{LCCS}^2 L'_{sL} + \dfrac{1}{C'_{sLCCS}}$	$\omega_{LCCS}^2 = \dfrac{L_{psLCCS}+L_{epLCCS}}{L_{psLCCS} L_{epLCCS} C_{ppLCCS}}$ $= \dfrac{1}{L_m(C_{epLCCS}+C'_{esLCCS})}$	$G_{LCCS} = \left(-\dfrac{L_{epLCCS}}{L_{psLCCS}}\right)\left(-\dfrac{C_{epLCCS}}{C'_{esLCCS}}\right)$
LCC-P	$-\omega_{LCCP}^2 L_{epLCCP} + \dfrac{1}{C_{epLCCP}} = -\omega_{LCCP}^2 L_{pL} + \dfrac{1}{C_{psLCCP}}$	$\omega_{LCCP}^2 = \dfrac{L_{psLCCP}+L_{epLCCP}}{L_{psLCCP} L_{epLCCP} C_{ppLCCP}}$ $= \dfrac{L_m + L'_{LS}}{L_m L'_{LS} C_{epP}}$	$G_{LCCP} = \left(-\dfrac{L_{epLCCP}}{L_{psLCCP}}\right)\dfrac{L_m + L'_{sL}}{L_m}$

TABLE II
LOAD-INDEPENDENT INPUT ZPA OPERATIONS IN CV MODES OF THE S-P, S-SP, LCC-S, AND LCC-P TOPOLOGIES.

	Resonant conditions for achieving load-independent ZPA	Input impedance Z_{inx}
S-P	$(L_m + L'_{sL})^2 C'_{spSP} = L_m L'_{sL} C_{epSP}$	
S-SP	$(L_m + L'_{esSSP})^2 C'_{spSSP} = L_m L'_{esSSP} C_{epSSP}$	$\dfrac{R'_{ac}}{|G_x|^2}$
LCC-S	$L_{psLCCS} C_{ppLCCS} C'_{esLCCS} = L_{epLCCS} C_{epLCCS} C'_{esLCCS} + L_{epLCCS} C_{epLCCS}^2$	
LCC-P	$L'_{sL} L_m L_{psLCCP} C_{epLCCP} + (L'_{sL}+L_m)^2 L_{epLCCP} C'_{spLCCP} = (L_m^2 + (L'_{sL}+L_m)L_{epLCCP}) L_{psLCCP} C_{ppLCCP}$	

(V_{abSP}, V_{abSSP}, and V_{abLCCS}) are in phase with the input voltage (V_{AB}), however, V_{abSS} and V_{abLCCP} lag V_{AB} by 180 degrees. In addition, the voltage gain of the S-P topology (G_{SP}) is equal to the reciprocal of the coupling coefficient, that is $G_{SP}=1/k$. So the S-P compensation network can be applied to achieve high voltage output application owing to the fact of low coupling coefficient in IPT system.

B. Load-independent ZPA operating condition in CV mode

The ZPA operating condition between the input voltage and current of the resonant tank can minimize the reactive current and ensure ZVS for the MOSFET-based inverter. So, under the conditions of achieving load-independent voltage transfer characteristics, load-independent input ZPA operations of the S-S, S-P, S-SP, LCC-S, LCC-P, and double-sided LCC topologies are analyzed in this section. Here, the double-sided LCC topology is also analyzed in detail.

From Fig. 3, the input impedance of the double-sided LCC topology Z_{inDLCC} is given by (4), shown at the bottom of the previous page. In (4), the "||" represents "parallel circuits" sign. The ZPA condition is achieved when the imaginary component of the input impedance $\mathrm{Im}\,(Z_{inDLCC})$ equals ze-ro. In this case, the resonant condition for achieving load-independent ZPA is given by (5), also shown at the bottom of the previous page. Under the conditions of (5), the purely resistive input impedance R_{inDLCC} is given by

$$R_{inDLCC} = \mathrm{Re}\,(Z_{inDLCC}) = \frac{R'_{ac}\,(L_{psDLCC}C'_{esDLCC}L'_{esDLCC})^2}{(L_{epDLCC}C_{epDLCC}L'_{ssDLCC})^2}$$

$$= \frac{R'_{ac}}{|G_{DLCC}|^2} \tag{6}$$

Similarly, the load-independent input ZPA operating conditions for the S-P, S-SP, LCC-S, and LCC-P topologies are also calculated, which are tabulated in Tab. II. It can be observed that the input impedance of all compensation topologies are expressed regularly as $R'_{ac}/|G_x|^2$ (the voltage transfer ratio G_x has been derived in Tab. I). Additionally, it should be pointed out that there is no ZPA condition for the S-S compensation topology in load-independent voltage output mode. This calculated result is compliance with the analysis in [9], [15]. So, the S-S topology is not listed in Tab. II and will not be analyzed in the next section.

III. QUANTITATIVE SENSITIVITY ANALYSES OF PARAMETRIC UNCERTAINTY IN IPT SYSTEMS

According to the analysis in the last section, both the load-independent output voltages and load-independent ZPA operations for the S-P, S-SP, LCC-S, LCC-P, and double-sided LCC compensation networks are achieved when ignoring the ESR (Equivalent Series Resistance) of the compensation components. However, the variation of the load resistance has negative effect on the output voltage and input impedance when considering the ESRs. Furthermore, these features are also affected by the variations of the frequency and misalignment between the primary and secondary coils. This section first designs the system parameters of all topologies that achieve load-independent voltage output and load-independent ZPA operation simultaneously based on section II. Then, the parameters sensitivity to the key performance factors when considering the ESRs will be analyzed.

A. parameters design

The self-inductances of the primary and secondary coils for all topologies are designed to be equal to 120 μH and the coupling factor of the transformer without misalignment is 0.2. The system operating frequency is 85 kHz. The input DC voltage is equal to 200 V. And the rated voltage transfer ratio is designed to 1.5 to achieve output voltage of 300 V, which can be used to charge the EVs or the automated guided vehicles (AGVs). Then according to the analyses in section II-A and II-B, the system specifications of the S-SP, LCC-S, LCC-P, and double-sided LCC compensated IPT systems are designed and tabulated in Tab. III. For the S-P compensation topology, however, the voltage transfer ratio is always equal to the reciprocal of the coupling coefficient ($G_{\mathrm{SP}}=1/k$) from

TABLE III
SYSTEM SPECIFICATION AND PARAMETERS.

|	Parameters	Value
	Operating frequency	85 kHz
	Input DC voltage (V_{dc})	200 V
	Voltage transfer ratio	1.5
	Output power	3-kW
Loosely Coupled Transformer	Self-inductance in primary side (L_{pS})	120 μH
	Self-inductance in secondary side (L_{sS})	120 μH
	Rated coupling coefficient (k_{o})	0.2
S-SP	Compensation capacitor in primary side C_{psSSP}	33.71 nF
	Series compensation capacitor in secondary side C_{ssSSP}	41.74 nF
	Parallel compensation capacitor in secondary side C_{spSSP}	97.39 nF
LCC-S	Compensation inductance in primary side L_{psLCCS}	40.58 μH
	Parallel compensation capacitor in primary side C_{ppLCCS}	219.12 nF
	Series compensation capacitor in primary side C_{psLCCS}	33.71 nF
	Series compensation capacitor in secondary side C_{ssLCCS}	20.00 nF
LCC-P	Compensation inductance in primary side L_{psLCCP}	151.92 μH
	Parallel compensation capacitor in primary side C_{ppLCCP}	100.00 nF
	Series compensation capacitor in primary side C_{psLCCP}	50.36 nF
	Parallel compensation capacitor in secondary side C_{spLCCP}	42.55 nF
Double-sided LCC	Compensation inductances in primary and secondary sides L_{psDLCC}, L_{ssDLCC}	28.82 μH, 54.66 μH
	Parallel compensation capacitors in primary and secondary sides C_{ppDLCC}, C_{spDLCC}	157.46 nF, 120.79 nF
	Series compensation capacitors in primary and secondary sides C_{psDLCC}, C_{ssDLCC}	50 nF, 50 nF
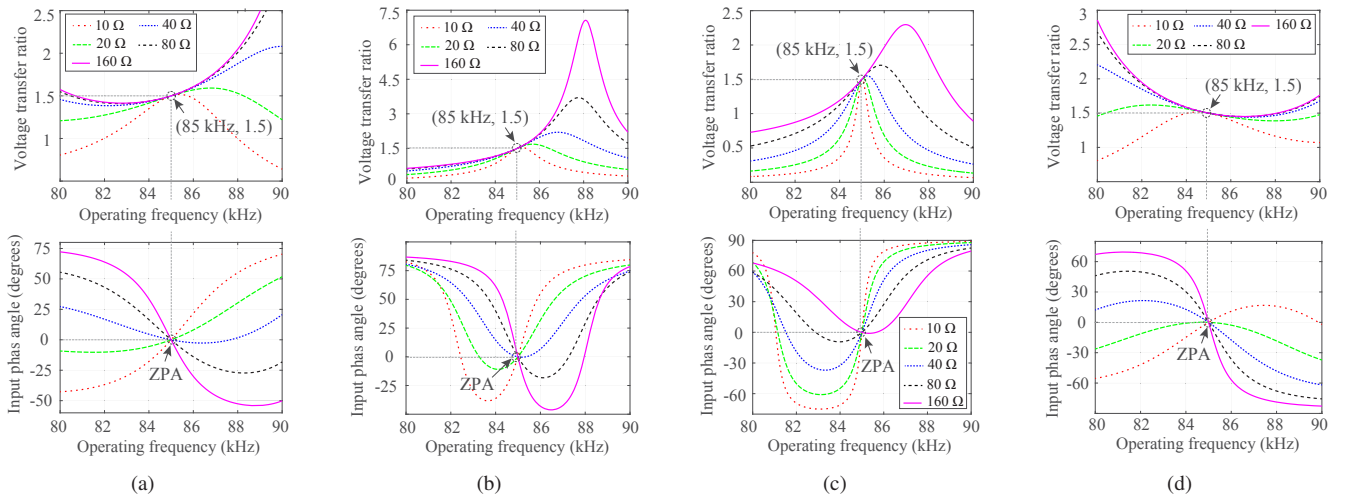
Fig. 5. Voltage transfer ratio and phase angle of the input impedance for (a) S-SP, (b) LCC-S, (c) LCC-P, and (d) double-sided LCC topologies versus operating frequency when the ESRs of the compensation components are neglected.
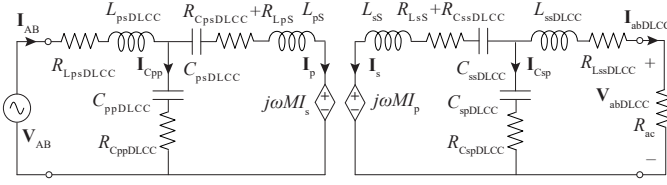
Fig. 6. Double-sided LCC compensation topology with resonant circuit losses included.

Tab. I. The designed coupling coefficient is 0.2. It means G_{SP} is equal to 5. For the consistency of the study, so, the S-P topology will not be analyzed in the later section. However, it should be pointed out that the S-P compensation topology can be applied to achieve high output voltage owing to the small coupling coefficient in IPT systems.

Substituting the designed parameters into (3), (6), Tab. I, and Tab. II, the voltage transfer ratio and the phase angle of the input impedance $[\theta_{\mathrm{in}x} = \frac{180°}{\pi}\tan^{-1}\frac{\mathrm{Re}(Z_{\mathrm{in}x})}{\mathrm{Im}(Z_{\mathrm{in}x})}]$ for the S-SP, LCC-S, LCC-P, and double-sided LCC topologies with different loading conditions can be plotted, which are shown in Fig. 5(a), 5(b), 5(c), and 5(d). It can be seen that load-independent voltage transfer ratio of 1.5 and load-independent ZPA operation are achieved for all compensation topologies when the IPT system operates at 85 kHz, which match well with the theoretical analysis.

B. Quantitative sensitivity analysis

Based on the designed parameters for the loosely coupled transformer and all compensation networks, the key performance factors versus the variation of the parameters are analyzed when considering the ESRs both of the inductors and capacitors. The double-sided LCC compensation topology is also taken as an example to analyze the sensitivity in detail, which is shown in Fig. 6. R_{LpsDLCC}, R_{CppDLCC}, R_{CpsDLCC}, R_{LpS}, R_{LsS}, R_{CssDLCC}, R_{CspDLCC}, and R_{LssDLCC} are the ESRs of the corresponding passive components. The input impedance (Z_{inDLCC}), the phasor form of the currents on primary and secondary coils ($\mathbf{I}_\mathrm{p}$ and $\mathbf{I}_\mathrm{s}$), voltage transfer ratio (G_{DLCC}), and transfer efficiency η_{DLCC} are calculated in (7), (9), (10), (11), and (12), respectively. In addition, the analysis for the S-SP, LCC-S, and LCC-P topologies are similar to that of the double-sided LCC topology and are therefore omitted.

$$Z_{\mathrm{inDLCC}} = \left(\frac{(\omega_{\mathrm{DLCC}}M)^2}{((R_{\mathrm{ac}} + Z_{\mathrm{s1}}) \parallel Z_{\mathrm{s2}}) + Z_{\mathrm{s3}}} + Z_{\mathrm{p3}}\right) \parallel Z_{\mathrm{p2}} + Z_{\mathrm{p1}} \quad (7)$$

where

$$Z_{\mathrm{s1}} = j\omega_{\mathrm{DLCC}}L_{\mathrm{ssDLCC}} + \frac{\omega_{\mathrm{DLCC}}L_{\mathrm{ssDLCC}}}{Q_{\mathrm{L}}}$$

$$Z_{\mathrm{s2}} = \frac{1}{(j\omega_{\mathrm{DLCC}}C_{\mathrm{spDLCC}})} + \frac{D_{\mathrm{F}}}{(\omega_{\mathrm{DLCC}}C_{\mathrm{spDLCC}})}$$

$$Z_{\mathrm{s3}} = j\omega_{\mathrm{DLCC}}L_{\mathrm{sS}} + \frac{(\omega_{\mathrm{DLCC}}L_{\mathrm{sS}})}{Q_{\mathrm{LCT}}}$$
$$+ \frac{1}{(j\omega_{\mathrm{DLCC}}C_{\mathrm{ssDLCC}})} + \frac{D_{\mathrm{F}}}{(\omega_{\mathrm{DLCC}}C_{\mathrm{ssDLCC}})}$$

$$Z_{\mathrm{p3}} = j\omega_{\mathrm{DLCC}}L_{\mathrm{pS}} + \frac{(\omega_{\mathrm{DLCC}}L_{\mathrm{pS}})}{Q_{\mathrm{LCT}}}$$
$$+ \frac{1}{(j\omega_{\mathrm{DLCC}}C_{\mathrm{psDLCC}})} + \frac{D_{\mathrm{F}}}{(\omega_{\mathrm{DLCC}}C_{\mathrm{psDLCC}})}$$

$$Z_{\mathrm{p2}} = \frac{1}{(j\omega_{\mathrm{DLCC}}C_{\mathrm{ppDLCC}})} + \frac{D_{\mathrm{F}}}{(\omega_{\mathrm{DLCC}}C_{\mathrm{ppDLCC}})}$$

$$Z_{\mathrm{p1}} = j\omega_{\mathrm{DLCC}}L_{\mathrm{psDLCC}} + \frac{\omega_{\mathrm{DLCC}}L_{\mathrm{psDLCC}}}{Q_{\mathrm{L}}} \quad (8)$$

in (8), Q_{L} and Q_{LCT} represent the quality factors of the compensation inductor and coil respectively, and D_{F} is the dissipation factor of the compensation capacitor.

$$\mathbf{I}_\mathrm{p} = \frac{\mathbf{V}_{\mathrm{AB}}}{Z_{\mathrm{inDLCC}}} - \frac{\mathbf{V}_{\mathrm{AB}} - \frac{\mathbf{V}_{\mathrm{AB}}}{Z_{\mathrm{inDLCC}}}Z_{\mathrm{p1}}}{Z_{\mathrm{p2}}} \quad (9)$$

$$\mathbf{I}_\mathrm{s} = \frac{\mathbf{V}_{\mathrm{AB}} - \frac{\mathbf{V}_{\mathrm{AB}}}{Z_{\mathrm{inDLCC}}}Z_{\mathrm{p1}} - \frac{\mathbf{V}_{\mathrm{AB}}}{Z_{\mathrm{inDLCC}}} - \frac{\mathbf{V}_{\mathrm{AB}} - \frac{\mathbf{V}_{\mathrm{AB}}}{Z_{\mathrm{inDLCC}}}Z_{\mathrm{p1}}}{Z_{\mathrm{p2}}}Z_{\mathrm{p3}}}{j\omega_{\mathrm{DLCC}}M} \quad (10)$$

$$G_{\mathrm{DLCC}} = \left|\frac{\mathbf{V}_{\mathrm{abDLCC}}}{\mathbf{V}_{\mathrm{AB}}}\right|$$
$$= \left|\frac{\frac{\mathbf{I}_\mathrm{s}Z_{\mathrm{s3}} + j\omega_{\mathrm{DLCC}}M\mathbf{I}_\mathrm{p}}{Z_{\mathrm{s2}}}(Z_{\mathrm{s2}} + Z_{\mathrm{s1}}) + \mathbf{I}_\mathrm{s}Z_{\mathrm{s1}}}{\mathbf{V}_{\mathrm{AB}}}\right| \quad (11)$$

$$\eta_{\mathrm{DLCC}} = \frac{P_{\mathrm{outDLCC}}}{P_{\mathrm{outDLCC}} + P_{\mathrm{lossDLCC}}} \quad (12)$$

in (12), the output power P_{outDLCC} and power loss P_{lossDLCC} are expressed by (13) and (14).

$$P_{\mathrm{outDLCC}} = \frac{\mathbf{V}_{\mathrm{abDLCC}}^2}{R_{\mathrm{ac}}} \quad (13)$$

In this paper, we consider the variations of the coupling, load, and frequency depending on the practical IPT application. The coupling coefficient k of the transformer is usually changed from 0.1 to 0.3 [29]. The equivalent ac resistance R_{ac} is roughly changed from 10 to 200 Ω [6] when the battery charging power was between 5% to 100% power. And

$$P_{\mathrm{lossDLCC}} = \left(\frac{\mathbf{V}_{\mathrm{AB}}}{Z_{\mathrm{inDLCC}}}\right)^2 \frac{\omega_{\mathrm{DLCC}}L_{\mathrm{psDLCC}}}{Q_{\mathrm{L}}} + \left(\frac{\mathbf{V}_{\mathrm{AB}} - \frac{\mathbf{V}_{\mathrm{AB}}}{Z_{\mathrm{inDLCC}}}Z_{\mathrm{p1}}}{Z_{\mathrm{p2}}}\right)^2 \frac{D_{\mathrm{F}}}{\omega_{\mathrm{DLCC}}C_{\mathrm{ppDLCC}}} + \mathbf{I}_\mathrm{p}^2\left(\frac{\omega_{\mathrm{DLCC}}L_{\mathrm{pS}}}{Q_{\mathrm{LCT}}} + \frac{D_{\mathrm{F}}}{\omega_{\mathrm{DLCC}}C_{\mathrm{psDLCC}}}\right)$$
$$+ \mathbf{I}_\mathrm{s}^2\left(\frac{\omega_{\mathrm{DLCC}}L_{\mathrm{sS}}}{Q_{\mathrm{LCT}}} + \frac{D_{\mathrm{F}}}{\omega_{\mathrm{DLCC}}C_{\mathrm{ssDLCC}}}\right) + \left(\frac{\mathbf{I}_\mathrm{s}Z_{\mathrm{s3}} + j\omega_{\mathrm{DLCC}}M\mathbf{I}_\mathrm{p}}{Z_{\mathrm{s2}}}\right)^2 \frac{D_{\mathrm{F}}}{\omega_{\mathrm{DLCC}}C_{\mathrm{ppDLCC}}}$$
$$+ \left(\frac{\mathbf{I}_\mathrm{s}(Z_{\mathrm{s2}} + Z_{\mathrm{s3}}) + j\omega_{\mathrm{DLCC}}M\mathbf{I}_\mathrm{p}}{Z_{\mathrm{s2}}}\right)^2 \frac{\omega_{\mathrm{DLCC}}L_{\mathrm{ssDLCC}}}{Q_{\mathrm{L}}} \quad (14)$$
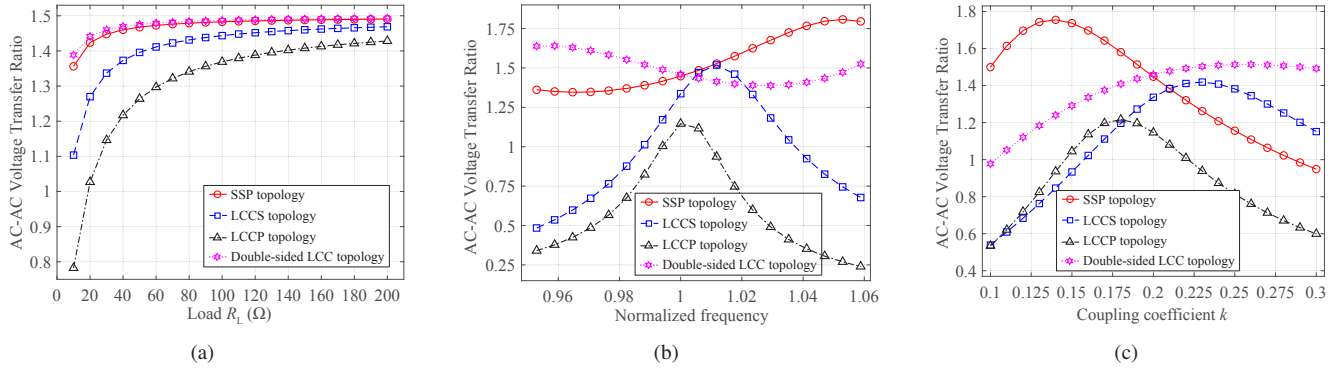
Fig. 7. Voltage transfer ratio of the S-SP, LCC-S, LCC-P, and double-sided LCC topologies versus (a) loading condition at 85 kHz and the coupling coefficient of 0.2, (b) normalized frequency at the load of 30 Ω and the coupling of 0.2, and (c) coupling coefficient at 85 kHz and the load of 30 Ω.
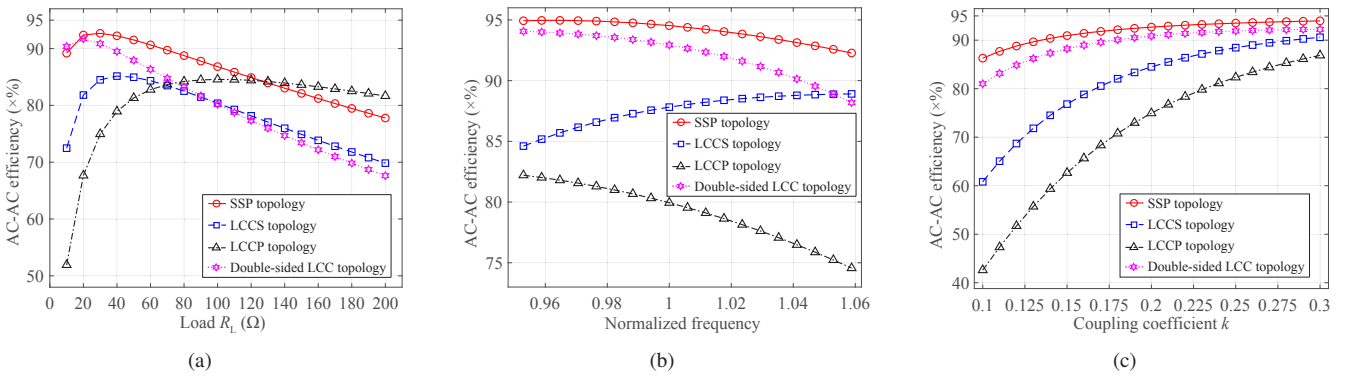

Fig. 8. Transfer efficiency of the S-SP, LCC-S, LCC-P, and double-sided LCC resonant tank circuits versus (a) loading condition at 85 kHz and the coupling coefficient of 0.2, (b) normalized frequency at the load of 30 Ω and the coupling of 0.2, and (c) coupling coefficient at 85 kHz and the load of 30 Ω.

the frequency ranges from 81.38-90 kHz according to the SAE J2954. The measured quality factor of the compensation inductors (Q_L) without ferrite and aluminum shielding is approximately 500, however, that of the primary and secondary coils with PC40 ferrite core and aluminum shielding (Q_{LCT}) is about 200. Then the corresponding parasitic resistances of the compensation inductors can be calculated by $R_L = \omega L/Q$, as well as that of the primary and secondary coils. In addition, double sided metallized polypropylene film capacitors with a dissipation factor (D_F) of 1.5 ‰ are chosen. So, the ESR of the compensation capacitor can be given by $R_C = D_F/(\omega C)$.

The voltage transfer ratio comparisons between S-SP, LCC-S, LCC-P, and double-sided LCC topologies in respect to the load, normalized frequency (the ratio of resonant frequency to operating frequency), and coupling factor are shown in Fig. 7(a), 7(b), and 7(c) respectively. Overall, the voltage transfer ratio of the double-sided LCC topology is the least sensitive to the variation of the load, frequency, and coupling, and followed by the S-SP topology. It means that the double-sided LCC topology are more suitable for achieving constant output voltage with independent of variation of all possible parameters in a closed-loop IPT system with a back-end DC/DC converter. Because higher efficiency, lower cost, and simple control algorithm can be achieved for a DC/DC converter with narrow output voltage range. In addition, the closer voltage transfer ratios of all topologies are to the ideal value (G_x=1.5) at light loads from Fig. 7(a).
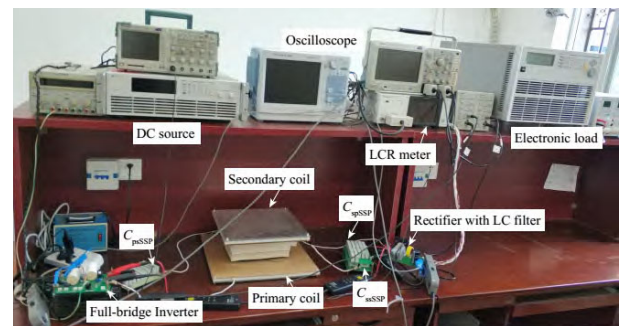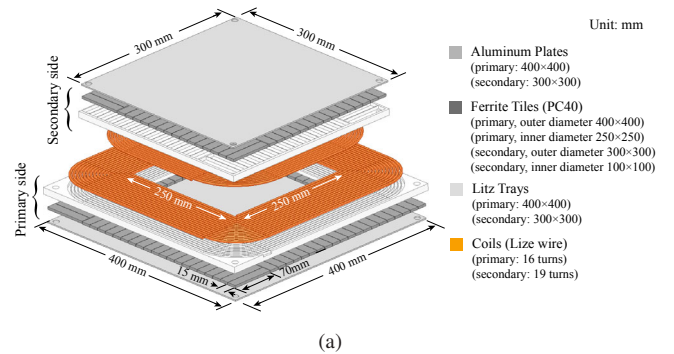

(a)

(b)

Fig. 9. (a) Loosely coupled transformer and (b) experiment prototype of the S-SP compensated IPT system.
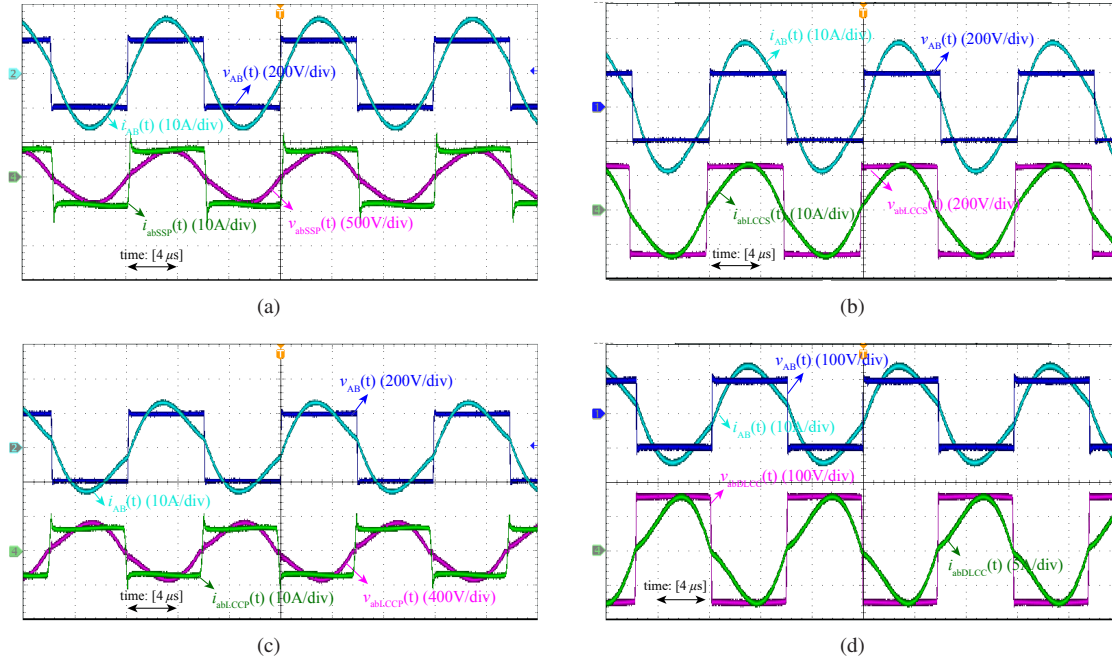
Fig. 10. Experimental results of the (a) S-SP, (b) LCC-S, (c) LCC-P, and (d) double-sided LCC compensated IPT systems at $k = 0.2$ and $R_L = 30\Omega$.

The simulated AC-AC efficiencies of the S-SP, LCC-S, LCC-P, and double-sided LCC compensation topologies are shown in Fig. 8. It can be seen that the efficiency of the S-SP compensation network is almost superior over a wide range of load (except at the very light load condition) and over the entire of coupling and frequency. In addition, from Fig. 8(c), the larger the coupling coefficient is, the higher the efficiencies for all topologies are achieved. The light load efficiency is a very important figure of merit (FoM) in wireless EV (electric vehicle) charging application. As is seen in Fig. 8(a), the LCC-P architecture has higher and steady light-load performance.

IV. EXPERIMENTAL EVALUATION

To verify the theoretical analysis, 3-kW S-SP, LCC-S, LCC-P, and double-sided LCC compensated IPT prototypes are implemented. In which, unipolar coils with the shape of square are used for both primary and secondary sides and shown in Fig. 9(a). The air gap between the primary and secondary coils is approximately 80 mm. And the designed geometric parameters of the coils are shown in Fig. 9(a). The photograph of the S-SP compensated IPT system is shown in Fig. 9(b). The LCC-S, LCC-P, and double-sided LCC prototypes are similar to that of the S-SP compensated IPT system and are therefore omitted. Here, it should be pointed out that the capacitors bank are obtained by connecting combinations of multiple capacitors in series and parallel, which will make the difference between the equivalent theoretical value shown in Tab. III and the experimental value less than 0.5 nF and increase the equivalent value of permissible voltage of the capacitor group. In addition, the primary side power MOSFETs are IPW65R041CFD. And the antiparallel diode of the MOSFET and secondary side diode of the rectifier use IDP30E65D2.
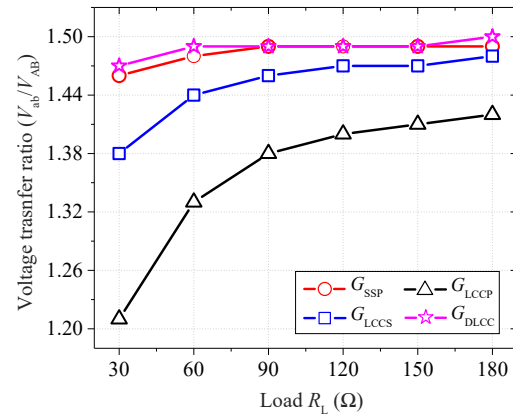

Fig. 11. Experimental results of the voltage transfer ratio for the S-SP, LCC-S, LCC-P, and double-sided LCC compensated IPT systems at the coupling coefficient of 0.2 and the operation frequency of 85 kHz.

The experimental waveforms of the S-SP, LCC-S, LCC-P, and double-sided LCC compensated IPT systems are shown in Fig. 10(a), 10(b), 10(c), and 10(d), respectively. It can be seen that the output voltage of the S-SP and LCC-S topologies, $v_{\mathrm{abSSP}}(t)$ and $v_{\mathrm{abLCCS}}(t)$, are nearly in phase with the input voltage, however, the $v_{\mathrm{abLCCP}}(t)$ and $v_{\mathrm{abDLCC}}(t)$ approximately lag the input voltage by 180 degrees, which match well with the analysis of (3) and Tab. I. In addition, the input currents of all topologies are almost in phase with the corresponding input voltages. It means that near ZPA conditions for all topologies are achieved. The little phase differences between the input current and voltage for all topologies are caused by the ESRs of the compensation components and harmonics of the input current. Last but not least, the output currents are in phase with the output voltages due to the diode rectifier action.
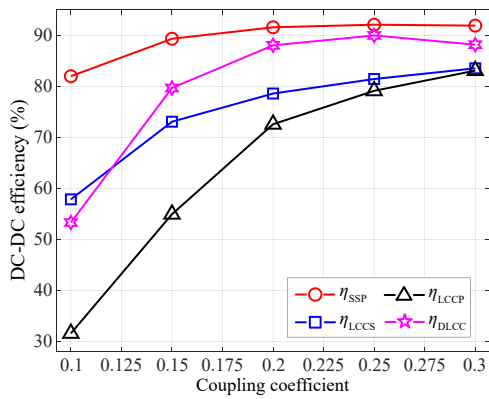
Fig. 12. Experimental efficiency of the S-SP, LCC-S, LCC-P, and double-sided LCC compensated IPT systems versus coupling coefficient at the load resistance of 30 Ω and the operation frequency of 85 kHz.
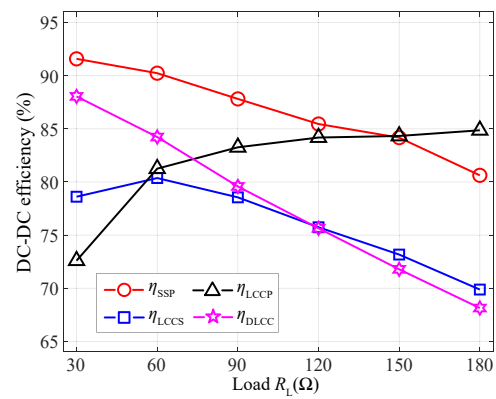

Fig. 13. Experimental efficiency of the S-SP, LCC-S, LCC-P, and double-sided LCC compensated IPT systems versus load resistance at the coupling coefficient of 0.2 and the operation frequency of 85 kHz.

Fig. 11 shows the measured ac voltage transfer ratios of the S-SP, LCC-S, LCC-P, and double-sided LCC compensated IPT systems. The higher voltage transfer ratio can be obtained at light loading condition for all topologies. And for the double-sided LCC and S-SP topologies, the voltage transfer ratios are less sensitive to changes in loads. The experimental results are consistent with the analytical results shown in Fig. 7(a).

Fig. 12 and 13 show the measured DC-DC efficiency of the S-SP, LCC-S, LCC-P, and double-sided LCC compensated IPT systems versus coupling and load respectively. It can be seen that the efficiency of the S-SP topology (η_{SSP}) is the least sensitive to the change in coupling factor compared with that of other systems. The larger the value of the load resistance, the higher the efficiency the LCC-P compensated IPT system (η_{LCCP}) can be achieved. Additional, when the IPT systems operate at a coupling coefficient of 0.2 and a load resistance of 30 Ω, the η_{SSP}, η_{LCCS}, and η_{LCCP}, and η_{DLCC} are 91.8 %, 78.6 %, 72.6 %, and 88.1 %, respectively.

V. CONCLUSION

In this paper, the sensitivity of the inevitable variation of the parameters to the voltage transfer ratio and transfer efficiency for all voltage-fed compensation topologies in IPT system are investigated. The theoretical analysis and experimental results of the 3-kW S-S, S-P, S-SP, LCC-S, LCC-P, and double-sided LCC compensated IPT systems show that:

1) All voltage-fed compensation topologies in IPT system can be designed to achieve the load-independent voltage transfer ratio.

2) For the S-P resonant topology, the load-independent voltage transfer ratio is always equal to the reciprocal of the coupling coefficient. It means the S-P compensation topology can be applied to get high output voltage owing to the low coupling coefficient in wireless charging system.

3) Load-independent ZPA operation in CV mode can be achieved for the S-P, S-SP, LCC-S, LCC-P, and double-sided LCC compensation topologies, except the S-S topology. And the input impedance for all analyzed topologies are expressed as $R'_{\mathrm{ac}}/|\mathbf{G}_x|^2$ ($\mathbf{G}_x$ represents

the voltage transfer ratio of different compensation topologies).

4) When considering the ESRs, the following conclusions can be made based on the parameter sensitivity analysis: (a) The double-sided LCC is the most robust topology to obtain approximate constant voltage output and have the minimum voltage error between the experimental results and the designed value compared with other topologies. So double-sided LCC topology can be used to achieve constant voltage output in a closed-loop IPT system to minimize the power converter and control algorithm efforts. (b) The efficiency of the S-SP compensated IPT system is the least sensitive to changes over a wide load range and the full coupling coefficient range. (c) The larger the load resistance is, the higher the efficiency of the LCC-P compensated IPT system is achieved. (d) The efficiency increases as the coupling coefficient increases for all topologies.

REFERENCES

[1] S. Li and C. C. Mi, "Wireless Power Transfer for Electric Vehicle Applications," *IEEE J. Emerg. Sel. Topics Power Electron.*, vol. 3, no. 1, pp. 4-17, Mar. 2015.

[2] D. Patil, M. Mcdonough, J. Miller, B. Fahimi, and P. T. Balsara, "Wireless Power Transfer for Vehicular Applications: Overview and Challenges," *IEEE Trans. Transp. Electrif.*, vol. PP, no. 99, Dec. 2017.

[3] X. Qu, Y. Jing, H. Han, S.-C. Wong, and C. K. Tse, "Higher Order Compensation for Inductive-Power-Transfer Converters with Constant-Voltage or Constant-Current Output Combating Transformer Parameter Constraints," *IEEE Trans. Power Electron.*, vol. 32, no. 1, pp. 394-405, Jan. 2017.

[4] W. Zhang and C. C. Mi, "Compensation Topologies of High-Power Wireless Power Transfer Systems," *IEEE Trans. Veh. Technol.*, vol. 65, no. 6, pp. 4768-4778, Jun. 2016.

[5] X. Qu, H. Han, S.-C. Wong, C. K. Tse, and W. Chen, "Hybrid IPT Topologies with Constant Current or Constant Voltage Output for Battery Charging Applications," *IEEE Trans. Power Electron.*, vol. 30, no. 11, pp. 6329-6337, Nov. 2015.

[6] S. Li, W. Li, J. Deng, T. D. Nguyen, and C. C. Mi, "A Double-Sided LCC Compensation Network and Its Tuning Method for Wireless Power Transfer," *IEEE Trans. Veh. Technol.*, vol. 64, no. 6, pp. 2261-2273, Jun. 2017.

[7] Z. Li, C. Zhu, J. Jiang, K. Song, and G. Wei, "A 3-kW Wireless Power Transfer System for Sightseeing Car Supercapacitor Charge," *IEEE Trans. Power Electron.*, vol. 32, no. 5, pp. 3301-3316, May. 2017.

[8] R. Mai, Y. Chen, Y. Li, Y. Zhang, G. Cao, and Z. He, "Inductive Power Transfer for Massive Electric Bicycles Charging Based on Hybrid Topology Switching with a Single Inverter," *IEEE Trans. Power Electron.*, vol. 32, no. 8, pp. 5897-5906, Sep. 2017.

[9] Z. Huang, S.-C. Wong, and C. K. Tse, "Design of a Single-Stage Inductive-Power-Transfer Converter for Efficient EV Battery Charging," *IEEE Trans. Veh. Technol.*, vol. 66, no. 7, pp. 5808-5821, Jul. 2017.

[10] J. Hou, Q. Chen, Z. Zhang, S.-C. Wong, and C. K. Tse, "Analysis of Output Current Characteristics for Higher Order Primary Compensation in Inductive Power Transfer Systems," *IEEE Trans. Power Electron.*, vol. 33, no. 8, pp. 6807-6821, Aug. 2018.

[11] X. Qu, W. Zhang, S.-C. Wong, and C. K. Tse, "Design of a Current-Source-Output Inductive Power Transfer LED Lighting System," *IEEE J. Emerg. Sel. Topics Power Electron.*, vol. 3, no. 1, pp. 306-314, Mar. 2015.

[12] W. Zhang, S.-Chung Wong, C. K. Tse, and Q. Chen, "Load-Independent Duality of Current and Voltage Outputs of a Series- or Parallel-Compensated Inductive Power Transfer Converter with Optimized Efficiency," *IEEE J. Emerg. Sel. Topics Power Electron.*, vol. 3, no. 1, pp. 306-314, Mar. 2015.

[13] V.-B. Vu, D.-H. Tran, and W. Choi, "Implementation of the Constant Current and Constant Voltage Charge of Inductive Power Transfer Systems with the Double-Sided LCC Compensation Topology for Electric Vehicle Battery Charge Applications," *IEEE Trans. Power Electron.*, vol. PP, no. 99, Oct. 2017.

[14] J. Lu, G. Zhu, D. Lin, S. C. Wong, and Jin Jiang, "Load-Independent Voltage and Current Transfer Characteristics of High-Order Resonant Network in IPT System," *IEEE J. Emerging. Sel. Topics Power Electron.*, vol. 7, no. 1, pp. 422-436, Mar. 2019.

[15] W. Zhang, S.-C. Wong, C. K. Tse, and Q. Chen, "Design for Efficiency Optimization and Voltage Controllability of Series-Series Compensated Inductive Power Transfer Systems," *IEEE Trans. Power Electron.*, vol. 29, no. 1, pp. 191-200, Jan. 2014.

[16] W. Zhang, S.-C. Wong, C. K. Tse, and Q. Chen, "Analysis and Comparison of Secondary Series- and Parallel-Compensated Inductive Power Transfer Systems Operating for Optimal Efficiency and Load-Independent Voltage-Transfer Ratio," *IEEE Trans. Power Electron.*, vol. 29, no. 6, pp. 2979-2990, Jun. 2014.

[17] J. Hou, Q. Chen, X. Ren, X. Ruan, S.-C. Wong, and C. K. Tse, "Precise Characteristics Analysis of Series/Series-Parallel Compensated Contactless Resonant Converter," *IEEE J. Emerg. Sel. Topics Power Electron.*, vol. 3, no. 1, pp. 101-110, Mar. 2015.

[18] Y. Wang, Y. Yao, X. Liu, and D. Xu, "S/CLC Compensation Topology Analysis and Circular Coil Design for Wireless Power Transfer," *IEEE Trans. Transp. Electrif.*, vol. 3, no. 2, pp. 496-507, Jun. 2017.

[19] Y. H. Sohn, B. H. Choi, G.-H. Cho, and C. T. Rim, "Gyrator-Based Analysis of Resonant Circuits in Inductive Power Transfer Systems," *IEEE Trans. Power Electron.*, vol. 31, no. 10, pp. 6824-6843, Oct. 2016.

[20] N. Liu and T. G. Habetler, "Design of a Universal Inductive Charger for Multiple Electric Vehicle Models," *IEEE Trans. Power Electron.*, vol. 30, no. 11, pp. 6378-6390, Nov. 2015.

[21] Y. Wang, G. Shi, Y. Yao, J. M. Alonso, W. Guo, X. Liu, and D. Xu, "A Double-T-Type Compensation Network and Its Tuning Method for IPT System," *IEEE Trans. Ind. Appl.*, vol. 53, no. 5, pp. 4757-4767, 2017.

[22] W. Li, H. Zhao, J. Deng, S. Li, and C. C. Mi, "Comparison Study on SS and Double-Sided LCC Compensation Topologies for EV/PHEV Wireless Chargers," *IEEE Trans. Veh. Technol.*, vol. 65, no. 6, pp. 4429-4439, Jun. 2016.

[23] B. Esteban, M. S. Ahmed, and N. C. Kar, "A Comparative Study of Power Supply Architectures in Wireless EV Charging Systems," *IEEE Trans. Power Electron.*, vol. 30, no. 11, pp. 6408-6422, Nov. 2015.

[24] F. Lu, H. Hofmann, J. Deng, and C. C. Mi, "Output power and efficiency sensitivity to circuit parameter variations in double-sided LCC-compensated wireless power transfer system," in *Proc. IEEE Applied Power Electronics Conference and Exposition.*, Mar. 2015, pp. 507-601.

[25] H. Wang and F. Blaabjerg, "Reliability of Capacitors for DC-Link Applications in Power Electronic Converters‖An Overview," *IEEE Trans. Ind. Appl.*, vol. 50, no. 5, pp. 3569-3578, Feb. 2014.

[26] G. Buja, M. Bertoluzzo, and H. K. Dashora "Lumped Track Layout Design for Dynamic Wireless Charging of Electric Vehicles," *IEEE Trans. Ind. Electron.*, vol. 63, no. 10, pp. 6631-6640, Oct. 2016.

[27] C.-Y. Huang, J. E. James, and G. A. Covic, "Design Considerations for Variable Coupling Lumped Coil Systems," *IEEE Trans. Power Electron.*, vol. 30, no. 2, pp. 680-689, Feb. 2015.

[28] R. L. Steigerwald, "A comparison of half-bridge resonant converter topologies," *IEEE Trans. Power Electron.*, vol. 3, no. 2, pp. 174 - 182, Apr. 1988.

[29] A. Kamineni, G. A. Covic, and J. T. Boys, "Analysis of Coplanar Intermediate Coil Structures in Inductive Power Transfer Systems," *IEEE Trans. Power Electron.*, vol. 30, no. 11, pp. 6141-6154, Dec. 2015.

[30] K. Song, Z. Li, J. Jiang, and C. Zhu, "Constant Current/Voltage Charging Operation for SeriesSeries and SeriesParallel Compensated Wireless Power Transfer Systems Employing Primary-Side Controller," *IEEE Trans. Power Electron.*, vol. 33, no. 9, pp. 8065-8080, Sept. 2018.

Jianghua Lu was born in Hubei, China, in 1989. He received the M.Sc. degree from the Wuhan University of Technology in 2016. He is currently pursuing the Ph.D. degree in electrical engineering at Wuhan University of Technology. In 2018, he received the funding from China Scholarship Council, and became a joint Ph.D. student in the Department of Electrical and Computer Engineering, San Diego State University, San Diego, CA, USA.

His current research interests include inductive power transfer and resonant converters.

Guorong Zhu (M'11-SM'15) was born in Hunan, China. She received the Ph.D. degree in electrical engineering from the Huazhong University of Science and Technology, Wuhan, China, in 2009.

From 2002 to 2005, she was a Lecturer with the School of Electrical Engineering, Wuhan University of Science and Technology, Wuhan. From 2009 to 2011, she was a Research Assistant/Research Associate in the Department of Electronic and Information Engineering, Hong Kong Polytechnic University, Kowloon, Hong Kong. She is currently an Associate Professor with the School of Automation, Wuhan University of Technology, Wuhan. Her main research interests are focused on wireless power transfer and the reliability of power electronics systems.

Huai Wang (M'12-SM'17) received the B.E. degree in electrical engineering, from Huazhong University of Science and Technology, Wuhan, China, in 2007 and the Ph.D. degree in power electronics, from the City University of Hong Kong, Hong Kong, in 2012. He is currently an Associate Professor at the Center of Reliable Power Electronics (CORPE), Aalborg University, Aalborg, Denmark. He was a Visiting Scientist with the ETH Zurich, Switzerland, from Aug. to Sep. 2014, and with the Massachusetts Institute of Technology (MIT), USA, from Sep. to Nov. 2013. He was with the ABB Corporate Research Center, Switzerland, in 2009. His research addresses the fundamental challenges in modelling and validation of power electronic component failure mechanisms, and application issues in system-level predictability, condition monitoring, circuit architecture, and robustness design.

Dr. Wang received the Richard M. Bass Outstanding Young Power Electronics Engineer Award from the IEEE Power Electronics Society in 2016, and the Green Talents Award from the German Federal Ministry of Education and Research in 2014. He is currently the Chair of IEEE PELS/IAS/IE Chapter in Denmark. He serves as an Associate Editor of IET Power Electronics, IET Electronics Letters, IEEE JOURNAL OF EMERGING AND SELECTED TOPICS IN POWER ELECTRONICS, and IEEE TRANSACTIONS ON POWER ELECTRONICS.

Fei Lu (S'12-M'17) received the B.S. and M.S. degree from Harbin Institute of Technology, Harbin, China, in 2010 and 2012, respectively, and the PhD degree from University of Michigan, Ann Arbor, Michigan, USA, in 2017, all in electrical engineering.

He is currently an assistant professor in the Department of Electrical and Computer Engineering in Drexel University, Philadelphia, PA, USA. His research topic focuses on power electronics and the application of electric vehicle charging.

Jin Jiang (S'85-M'87-SM'94-F'17) received the Ph.D. degree in electrical engineering from the University of New Brunswick, Fredericton, NB, Canada, in 1989. Since 1991, he has been with the Department of Electrical and Computer Engineering, The University of Western Ontario, London, ON, Canada, where he is currently a Senior Industrial Research Chair Professor. His research interests include fault-tolerant control of safety-critical systems, advanced control of electrical power plants, and power systems involving renewable energy resources.

He is a Fellow of the Canadian Academy of Engineering. He is also a member of the International Electrotechnical Commission 45A subcommittee to develop industrial standards on instrumentation and control for nuclear facilities. He also works closely with the International Atomic Energy Agency on modern control and instrumentation for nuclear power plants.

Chunting Chris Mi (S'00-A'01-M'01-SM'03-F'12) received the B.S.E.E. and M.S.E.E. degrees in electrical engineering from Northwestern Polytechnical University, Xi'an, China, and the Ph.D. degree in electrical engineering from the University of Toronto, Toronto, Ontario, Canada, in 1985, 1988, and 2001, respectively.

He is a Professor and chair of electrical and computer engineering and the Director of the Department of Energy (DOE) -funded Graduate Automotive Technology Education (GATE) Center for Electric Drive Transportation, San Diego State University, San Diego, USA. Prior to joining SDSU, he was with University of Michigan, Dearborn from 2001 to 2015.